Electron tunneling through a hybrid superconducting-normal mesoscopic junction under microwave radiation

Argo Nurbawono,[1] Yuan Ping Feng,[1] and Chun Zhang[1,2,*]
[1]*Department of Physics, National University of Singapore, 2 Science Drive 3, Singapore 117542, Singapore*
[2]*Department of Chemistry, National University of Singapore, 3 Science Drive 3, Singapore 117543, Singapore*
(Received 23 November 2009; published 30 July 2010)

We present a theoretical analysis for electron tunneling through a hybrid superconducting-normal mesoscopic junction consisting of a superconducting electrode, a two-level quantum dot, and a normal electrode under single mode microwave radiation. Using nonequilibrium Green's-function formalism, we incorporate Floquet basis in the Nambu space and solve the Green's function with finite matrix truncation to obtain the transport properties numerically. We studied the effects of photon-induced single-level oscillations and quantum transition between levels on the time-averaged current-voltage (*I-V*) characteristics of the system. For quantum dot with a single localized level, the main dc resonance remains unchanged regardless of the frequency and amplitude of the radiation, and a series of secondary resonances due to multiphoton processes are present. For quantum dot with two localized levels, the sole effects from the transitions between levels produce splitting on the main dc resonance at Rabi frequency proportional to the coupling. This provides the possibility for experimental inference of the interlevel coupling strength of the driven resonant tunneling system from the bias voltage energy difference between the split resonances in the *I-V* curve.

DOI: 10.1103/PhysRevB.82.014535 PACS number(s): 74.50.+r, 73.23.−b, 74.78.Na, 85.25.−j

I. INTRODUCTION

Nonequilibrium electron tunneling through a mesoscopic junction consisting of a nanoscale quantum dot in the center and two metal electrodes is a central issue in our understanding of mesoscopic electronic devices. In normal quantum dot junctions for which two electrodes are normal, electron tunneling through the quantum dot can be understood as the scattering of Bloch waves of electrons in two leads by localized orbitals in the quantum dot. When the coupling between the center quantum dot and two electrodes is weak, the scattering problem can be solved with nonequilibrium Green's-function (NEGF) techniques.[1] For strong-coupling cases like molecular junctions for which the center molecule is usually covalently bonded to two electrodes, the first-principles method combining density-functional theory and the aforementioned NEGF techniques proved to be powerful in solving the electron-tunneling problem.[2] When at least one of electrodes is superconducting, the electron tunneling through the quantum dot system is governed by Andreev reflections[3–5] which is completely different from junction with normal electrodes. In this case, in order to properly describe the formation of Cooper pairs in superconducing leads, Green's functions need to be expressed in 2×2 Nambu space. In literature, several theoretical approaches based on NEGF for electron tunneling through superconducting junctions have been proposed and successfully applied to different types of systems.[6–9]

Electron tunneling through a superconducting quantum dot system under laser or microwave fields represents another interesting and fruitful research direction. Experimentally, it is common to use laser fields focused on to the center region of the superconducting junction to study the phenomenon of so-called Shapiro steps.[10–12] Theoretically, the inclusion of the electron-photon interactions in superconducting junctions introduces extra time dependence in the superconducting phase due to the electromagnetic oscillations[12] that needs to be carefully dealt with. In the field of quantum computing, superconducting qubits constructed from Josephson junction had been proposed,[13] and measurements as well as theoretical discussions on these qubit states with photons interactions have been discussed in many papers.[14] As to *I-V* characteristics of a quantum dot coupled with two superconducting electrodes, previous theoretical studies based on NEGF techniques have focused on either single-level quantum dot system[9] or the junction for which two electrodes are connected by a featureless vacuum barrier.[12]

In this paper we shall consider using semiclassical microwave fields to study a system which consists of a superconducting electrode, a two-level quantum dot, and a normal electrode (SNN). The central aim is to build a method to study the effects of photon-induced transition between different levels in the center dot on electron tunneling through the superconducting junction which has never been discussed before. In this work, we focus on the weak-coupling regime and for simplicity neglect Coulomb interactions between electrons in the center dot as previous studies did.[7,9,15] Although the method we proposed here is for noninteracting electrons, i.e., in the absence of strong correlations, it serves as a convenient starting point in our understanding for further study in more complicated correlated transport systems. Prior discussions on a similar system was due to Sun *et al.*,[9] who considered the case of the single-level quantum dot and solved NEGF using Bessel functions. While Bessel basis provides analytical solutions for single-level quantum dot, it prohibits seamless extensions to multilevel quantum dots to cater interlevel transitions between them. On the other hand, Floquet basis[16] enables more flexible modeling of interlevel transitions, and its incorporation into NEGF and Nambu space is just as straight forward. We shall incorporate the Floquet basis into NEFG formalism in this paper, and discuss the separate effects of photon-induced independent energy-

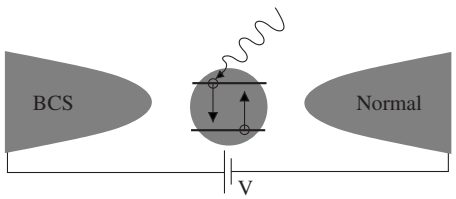

FIG. 1. Diagram of the quantum dot system with two localized levels coupled to the electrodes under dc bias V. The left electrode is superconducting governed by the BCS model and the right electrode is a normal conductor. Single mode microwave radiation stimulates Rabi oscillations between localized levels in the quantum dot, affecting its transport properties.

level oscillations and the interlevel transition dynamics.

Apart from standard quantum dot systems, some recent developments on superconducting quantum point contacts (QPCs) are worth mentioning for potential applications of the model we proposed. One such QPC is superconducting Nb-QPC produced using mechanically controlled break junction (MCBJ),[17] which was shown to have localized levels between the electrodes originating from the Nb dimer between the contacts.[18] New features in the subgap structure of current-voltage characteristics were found in the experiment when the whole junction is under a microwave field. Those new features cannot be understood by electron tunneling through a single-level quantum dot or featureless vacuum barrier. Since the coupling to the electrodes can be tuned piezoelectrically, such system may be finely engineered for a potential realization of our model. Ji *et al.*[19] recently proposed a well-designed experiment the use of superconducting scanning tunnel microscope to probe magnetic impurities on a substrate. Several localized impurity states inside the superconducting gap were identified and shown to have significant effects on Andreev reflections. Of course in both examples spins and Coulombic interaction would be important, nevertheless some qualitative pictures would be helpful to understand the basic ingredients of the complete physics involved in the process.

II. MODEL AND METHODS

The overall system's configuration is depicted in Fig. 1 and the Hamiltonian of the entire system can be written as

$$\hat{H}(t) = \hat{H}_L + \hat{H}_R + \hat{H}_T + \hat{H}_C(t), \tag{1}$$

where $\hat{H}_{L(R)}$ is the left (right) electrode Hamiltonian, $\hat{H}_T$ is the tunneling Hamiltonian, and $\hat{H}_C(t)$ is the quantum dot Hamiltonian. For the sake of clarity, the theoretical discussion is organized in two parts. In Sec. II A, we first focus on the Floquet treatment for the quantum dot Hamiltonian $\hat{H}_C(t)$ and its incorporation into the Green's-function formalism. In Sec. II B, time-averaged current is calculated by solving the Green's function and self-energies in Fourier space, employing Dyson and Keldysh formalisms. Standard NEGF formalism for transport models are adopted from Refs. 6–8 and 20.

A. Quantum dot under microwave radiation

We shall consider model Hamiltonian for a two-level quantum dot interacting with semiclassical external fields of frequency ω. Neglecting the Coulomb and spin interactions,

$$\hat{H}_C(t) = \sum_{i,\sigma} \left[\varepsilon_i + \frac{1}{2}eV + A\cos(\omega t) \right] c_{i\sigma}^{\dagger} c_{i\sigma} + \sum_{i \neq j,\sigma} B\cos(\omega t) c_{i\sigma}^{\dagger} c_{j\sigma}, \tag{2}$$

where $i,j=1,2$ denotes the unperturbed level index. A is the microwave field amplitude, and B is the coupling strength (hopping) between levels. We may also add a phase shift between them but it will not alter the ensuing method of solution. We shall set the left electrode potential to be zero ($V_L=0$, $V_R=\mathrm{V}$), thus the potential shift due to bias V on the localized level becomes $eV/2$, i.e., symmetric between contacts. As mentioned earlier, this model better suits those quantum dot systems where interactions are reasonably screened and effects from moderate interactions shall be discussed in Sec. III. $\hat{H}_C(t)$ is periodic in time and may be expanded in Fourier series,

$$\hat{H}_C(t) = \sum_n \hat{H}_C^{(n)} e^{-in\omega t}. \tag{3}$$

From the Floquet theory, the solutions of a two-level time-periodic Hamiltonian is given by two-component eigenfunctions ($\hbar=1$),[16]

$$\psi^{(p)}(t) = e^{-iq^{(p)}t}\phi^{(p)}(t), \tag{4}$$

where $q^{(p)}$ is the pth quasienergy and $\phi^{(p)}(t)$ is the time-periodic Floquet function which may also be expressed in Fourier series,

$$\phi^{(p)}(t) = \sum_n \phi_n^{(p)} e^{-in\omega t}, \tag{5}$$

where $\phi_n^{(p)}$ are also two-component functions spanned in terms of orthogonal basis functions of the unperturbed system. We have left out the spin degree of freedom in the solution because in this model the Hamiltonian is diagonal in spin. In order to transform the problem into a time-independent one, we normally rewrite the Schrödinger equation in terms of Floquet function $\phi^{(p)}(t)$,

$$\left[\hat{H}(t) - i\frac{d}{dt} \right] \phi^{(p)}(t) = q^{(p)}\phi^{(p)}(t) \tag{6}$$

and employ Floquet basis notations commonly adopted for such systems, which enable us to express the Schrödinger equation in Floquet-Fourier basis $|jn\rangle = |j\rangle \otimes |n\rangle$, where j (or i) is the system index and n is the Fourier index. In this notation the corresponding eigenvector for a given quasienergy $q_j^{(p)}$ is $|q_j\rangle_p$ and the Floquet coefficients are given by

$${}_p\langle in|q_j\rangle_{p'} = \phi_{i;n}^{(p)} \delta_{i,j}\delta_{p,p'}. \tag{7}$$

The eigenvalue problem can be written by inspection on the resulting Fourier components in Eq. (6) for any one pth quasistate set,[16]

$$\sum_j \sum_m \langle in|\hat{H}_F|jm\rangle\langle jm|q_k\rangle = q_k\langle in|q_k\rangle, \tag{8}$$

where the Floquet Hamiltonian is given by

$$\langle in|\hat{H}_F|jm\rangle = \hat{H}_{ij}^{(m-n)} - n\omega\delta_{i,j}\delta_{m,n}. \tag{9}$$

Now we can express our model Hamiltonian $\hat{H}_C$ in Floquet-Fourier basis, which simply takes the following form:

$$\hat{H}_C(t) = \begin{bmatrix} A & B \\ B & A \end{bmatrix}\frac{e^{-i\omega t}}{2} + \begin{bmatrix} \varepsilon_1 + \frac{1}{2}eV & 0 \\ 0 & \varepsilon_2 + \frac{1}{2}eV \end{bmatrix} + \begin{bmatrix} A & B \\ B & A \end{bmatrix}\frac{e^{i\omega t}}{2}$$

$$= \hat{H}_C^{(-1)}e^{-i\omega t} + \hat{H}_C^{(0)} + \hat{H}_C^{(1)}e^{i\omega t} \tag{10}$$

and the Floquet Hamiltonian (9) would be

$$\begin{bmatrix} \ddots & & & & & & & \\ \hat{H}_C^{(-1)} & \hat{E}^{(2)} & \hat{H}_C^{(1)} & & & & & \\ & \hat{H}_C^{(-1)} & \hat{E}^{(1)} & \hat{H}_C^{(1)} & & & & \\ & & \hat{H}_C^{(-1)} & \hat{E}^{(0)} & \hat{H}_C^{(1)} & & & \\ & & & \hat{H}_C^{(-1)} & \hat{E}^{(-1)} & \hat{H}_C^{(1)} & & \\ & & & & \hat{H}_C^{(-1)} & \hat{E}^{(-2)} & \hat{H}_C^{(1)} & \\ & & & & & & \ddots \end{bmatrix}, \tag{11}$$

finally the diagonal terms are given by

$$\hat{E}^{(n)} = \begin{bmatrix} \varepsilon_1 + \frac{1}{2}eV - n\omega & 0 \\ 0 & \varepsilon_2 + \frac{1}{2}eV - n\omega \end{bmatrix}. \tag{12}$$

After solving the Hamiltonian, the next quantity of interest for transport analysis is the retarded Green's function of the quantum dot, which can be written in Nambu space as

$$\mathbf{g}_{ij}^r(t,t_1) = -i\theta(t-t_1)\begin{bmatrix} \langle\{c_{i\uparrow}(t), c_{j\uparrow}^\dagger(t_1)\}\rangle & \langle\{c_{i\uparrow}(t), c_{j\downarrow}(t_1)\}\rangle \\ \langle\{c_{i\downarrow}^\dagger(t), c_{j\uparrow}^\dagger(t_1)\}\rangle & \langle\{c_{i\downarrow}^\dagger(t), c_{j\downarrow}(t_1)\}\rangle \end{bmatrix}. \tag{13}$$

Evaluation of each terms makes use the above results from the first quantization,[21]

$$\langle\{c_{i,\sigma}(t), c_{j,\sigma'}^\dagger(t_1)\}\rangle = \delta_{\sigma,\sigma'}\sum_p \psi_i^{(p)}(t)\psi_j^{(p)\star}(t_1). \tag{14}$$

Now we shall perform a double Fourier transform on the Green's functions whose purpose would be explained in the next section where we derive time-averaged current using NEGF formalism. The transformation shall take the form[8]

$$f_{mn}(\epsilon) = \frac{1}{2\pi}\int_{-\infty}^{\infty} dt_1 e^{-i(\epsilon+n\omega)t_1}\int_{-\infty}^{\infty} dt e^{i(\epsilon+m\omega)t} f(t,t_1). \tag{15}$$

After transformation the diagonal components of retarded Green's function in Nambu space are given by

$$\mathbf{g}_{ij;mn}^r(\epsilon)_{11} = \sum_p \frac{\phi_{i;m}^{(p)}\phi_{j;n}^{(p)\star}}{\epsilon + m\omega - q_i^{(p)} + i\eta}\delta(m-n-Q_{ij}^p),$$

$$\mathbf{g}_{ij;mn}^r(\epsilon)_{22} = \sum_p \frac{\phi_{i;m}^{(p)\star}\phi_{j;n}^{(p)}}{\epsilon + m\omega + q_i^{(p)} + i\eta}\delta(m-n+Q_{ij}^p). \tag{16}$$

The off-diagonal components in Nambu space are zero in this case due to orthogonal spin functions. The nonharmonic term Q_{ij}^p is the normalized quasienergy difference, $Q_{ij}^p = (q_i^{(p)} - q_j^{(p)})/\omega$ and this quantity can be either integer or noninteger. The delta functions in Eq. (16) are interpreted as

$$\delta(m-n\pm Q_{ij}^p) = \begin{cases} \delta_{m,n}\delta_{i,j} & \text{when } Q_{ij}^p \neq \text{integer} \\ \delta_{m,n\mp\nu} & \text{when } Q_{ij}^p = \text{integer } \nu. \end{cases} \tag{17}$$

In real calculations, the magnitude for the limit of the integer round up in taken to be in the same order of η in the denominator of Eq. (16). We have verified that larger or smaller value for this limit does not affect the results presented in this paper due to the fact that all these off-diagonal terms in Green's functions are orders of magnitudes smaller than the diagonal ones. We will see this more clearly in the discussion of *I-V* characteristics in the later section.

The products on the numerator of Eq. (16) make use the orthogonality of basis functions of the system, $\phi_{i;m}^{(p)}\phi_{j;n}^{(p)\star} = \Sigma_k \phi_{ik;m}^{(p)}\phi_{jk;n}^{(p)\star}$. In the case of a quantum dot with only one localized level ($\varepsilon_i = \varepsilon_0$ and $B=0$) the solution for $\hat{H}_C(t)$ is exact, given in terms of the Bessel function,[22]

$$\psi^{(p)}(t) = e^{-i(\varepsilon_0 + 1/2eV + p\omega)t}J_p(\alpha), \tag{18}$$

where $\alpha = A/\omega$ and the corresponding retarded Green's function after Fourier transform would be

$$\mathbf{g}_{mn}^r(\epsilon)_{11} = \delta_{m,n}\sum_p \frac{J_p(\alpha)J_p^\star(\alpha)}{\epsilon + (m-p)\omega - \varepsilon_0 - eV/2 + i\eta},$$

$$\mathbf{g}_{mn}^r(\epsilon)_{22} = \delta_{m,n}\sum_p \frac{J_p^\star(\alpha)J_p(\alpha)}{\epsilon + (m+p)\omega + \varepsilon_0 + eV/2 + i\eta},$$

which may be used to test the convergence against their Floquet basis counterparts as we shall demonstrate in the discussions of Sec. III.

B. Time-averaged current

Referring to Eq. (1), the terms $\hat{H}_L$, $\hat{H}_R$, and $\hat{H}_T$ are the following:

$$\hat{H}_L = \sum_{k,\sigma} \epsilon_{k\sigma}a_{Lk\sigma}^\dagger a_{Lk\sigma} + \sum_k \Delta(a_{Lk\downarrow}a_{L-k\uparrow} + a_{L-k\uparrow}^\dagger a_{Lk\downarrow}^\dagger), \tag{19}$$

$$\hat{H}_R = \sum_{k,\sigma} \epsilon_{k\sigma} a^\dagger_{Rk\sigma} a_{Rk\sigma}, \tag{20}$$

$$\hat{H}_T = \sum_{j,k,\sigma} t_{Lj}(a^\dagger_{Lk\sigma} c_{j\sigma} + c^\dagger_{j\sigma} a_{Lk\sigma}) + \sum_{j,k,\sigma} t_{Rj}(a^\dagger_{Rk\sigma} c_{j\sigma} + c^\dagger_{j\sigma} a_{Rk\sigma}). \tag{21}$$

$\hat{H}_L$ is the left electrode Hamiltonian governed by mean-field BCS theory. $\hat{H}_R$ is the right electrode Hamiltonian of the normal state. Operators $a^{(\dagger)}$ annihilate (create) particles on their respective electrodes. $\hat{H}_T$ is the tunneling Hamiltonian between both electrodes and the quantum dot, and the superconducting phase of the left electrode does not enter into the model because in this set up the time average current is independent of it. The current is derived from time derivative of number operator on one electrode,

$$I(t) = -e\left\langle \frac{d}{dt}\hat{N}_L(t) \right\rangle = ie\langle [\hat{N}_L(t), \hat{H}(t)] \rangle$$

$$= 2e\ \mathrm{Re}\sum_{i,k} \mathrm{Tr}\{\mathbf{G}^<_{i,Lk}(t,t)\mathbf{t}_{Li}\boldsymbol{\sigma}_z\}, \tag{22}$$

where $\mathbf{G}^<_{i,Lk}(t,t)$ and $\mathbf{t}_{Li}$ are defined as

$$\mathbf{G}^<_{j,Lk}(t,t_1) = i\begin{bmatrix} \langle a^\dagger_{Lk\uparrow}(t_1)c_{j\uparrow}(t)\rangle & \langle a_{L-k\downarrow}(t_1)c_{j\uparrow}(t)\rangle \\ \langle a^\dagger_{Lk\uparrow}(t_1)c^\dagger_{j\downarrow}(t)\rangle & \langle a_{L-k\downarrow}(t_1)c^\dagger_{j\downarrow}(t)\rangle \end{bmatrix}, \tag{23}$$

$$\mathbf{t}_{Lj} = \begin{bmatrix} t_{Lj} & 0 \\ 0 & -t^\star_{Lj} \end{bmatrix}, \tag{24}$$

and $\boldsymbol{\sigma}_z$ is the Pauli matrix. By writing the general time-ordered function of $\mathbf{G}^T_{i,Lk}(t,t_1)$ we can obtain a differential equation describing its equation of motion. In the nonequilibrium treatment, the real time variable is replaced with complex time and integration is then performed using contour integral. Subsequently Langreth's theorem of analytical continuation gives us the standard expression for $\mathbf{G}^<_{i,Lk}(t,t)$,

$$\mathbf{G}^<_{i,Lk}(t,t) = \sum_j \int dt_1 [\mathbf{G}^r_{ij}(t,t_1)\mathbf{t}^\star_{Lj}\mathbf{g}^<_{Lk}(t_1,t) + \mathbf{G}^<_{ij}(t,t_1)\mathbf{t}^\star_{Lj}\mathbf{g}^a_{Lk}(t_1,t)], \tag{25}$$

where the free Green's functions $\mathbf{g}^{<,a}_{Lk}$ belong to the left electrode. Green's function for BCS Hamiltonian has been solved and discussed in the literature using Bogoliubov transformations. We include the results in Eqs. (29) and (30) for completeness, where ρ^N is normal density of states (DOS), $f_L(\epsilon)$ is the Fermi-Dirac distribution function of the left electrode, and $\beta(\epsilon)$ is the complex BCS density of states,

$$\beta(\epsilon) = \frac{|\epsilon|}{\sqrt{\epsilon^2-\Delta^2}}\theta(|\epsilon|-\Delta) + \frac{\epsilon}{i\sqrt{\Delta^2-\epsilon^2}}\theta(\Delta-|\epsilon|). \tag{26}$$

We can write the current equation as in Eq. (31), where $\tilde{\boldsymbol{\Sigma}}(\epsilon)$ is defined as

$$\tilde{\boldsymbol{\Sigma}}(\epsilon) = \begin{bmatrix} 1 & -\Delta/\epsilon \\ -\Delta/\epsilon & 1 \end{bmatrix}. \tag{27}$$

The next step is to evaluate the Green's functions by solving self-energies $\boldsymbol{\Sigma}^{r/<}(t,t_1)$ required for the evaluation of $\mathbf{G}^{r/<}(t,t_1)$. Using the standard resonant-level model[20] the self-energy can be written as

$$\boldsymbol{\Sigma}^{r/<}_{L(R)ij}(t,t_1) = \sum_k \mathbf{t}^\star_{L(R)i}\mathbf{g}^{r/<}_{L(R)k}(t,t_1)\mathbf{t}_{L(R)j}, \tag{28}$$

$$\sum_k \mathbf{g}^r_{Lk}(t_1,t) = -i\theta(t_1-t)\int d\epsilon \rho^N \beta(\epsilon) e^{i\epsilon(t-t_1)}\begin{bmatrix} 1 & \Delta/\epsilon \\ \Delta/\epsilon & 1 \end{bmatrix}, \tag{29}$$

$$\sum_k \mathbf{g}^<_{Lk}(t_1,t) = i\int d\epsilon \rho^N f_L(\epsilon)\mathrm{Re}[\beta(\epsilon)] e^{i\epsilon(t-t_1)}\begin{bmatrix} 1 & \Delta/\epsilon \\ \Delta/\epsilon & 1 \end{bmatrix}, \tag{30}$$

$$I(t) = -2e\ \mathrm{Im}\sum_{i,j}\int_{-\infty}^{t} dt_1 \int \frac{d\epsilon}{2\pi} e^{i\epsilon(t-t_1)} \times \mathrm{Tr}\{\{\mathrm{Re}[\beta(\epsilon)]f_L(\epsilon)\mathbf{G}^r_{ij}(t,t_1) + \beta^\star(\epsilon)\mathbf{G}^<_{ij}(t,t_1)\}\Gamma_{Lij}(\epsilon)\tilde{\boldsymbol{\Sigma}}(\epsilon)\boldsymbol{\sigma}_z\}. \tag{31}$$

Since the current is time periodic, it can be expressed in Fourier series,

$$I(t) = \sum_n I_n e^{in\omega t} \tag{32}$$

and all the following analysis would be performed in Fourier space. Applying the double Fourier transform on to the self-energies yields

$$\boldsymbol{\Sigma}^r_{Lij;mn}(\epsilon) = -\delta_{m,n}\delta_{i,j}\frac{i}{2}\Gamma_{Lij}\beta(\epsilon+m\omega)\tilde{\boldsymbol{\Sigma}}(\epsilon+m\omega), \tag{33}$$

$$\boldsymbol{\Sigma}^<_{Lij;mn}(\epsilon) = \delta_{m,n}\delta_{i,j} i\Gamma_{Lij} f_L(\epsilon+m\omega)\mathrm{Re}[\beta(\epsilon+m\omega)]\tilde{\boldsymbol{\Sigma}}(\epsilon+m\omega), \tag{34}$$

$$\boldsymbol{\Sigma}^r_{Rij;mn}(\epsilon) = -\delta_{m,n}\delta_{i,j}\frac{i}{2}\Gamma_{Rij}\begin{bmatrix} 1 & 0 \\ 0 & 1 \end{bmatrix}, \tag{35}$$

$$\boldsymbol{\Sigma}^<_{Rij;mn}(\epsilon) = \delta_{m,n}\delta_{i,j} i\Gamma_{Rij}\begin{bmatrix} f^-_R & 0 \\ 0 & f^+_R \end{bmatrix}, \tag{36}$$

where $f^\pm_R = f_R(\epsilon + m\omega \pm eV)$. For simplicity we assume equal tunneling constants for each quantum dot levels, $t_{Li}=t_L$ and using wide bandwidth approximation[6] we can define the coupling strength $\Gamma_{Lij}(\epsilon)=2\pi\rho^N_L(\epsilon)t_{Li}t^\star_{Lj}=\Gamma_L$ independent of energy, as commonly adopted. The self-energy is assumed not to introduce level mixing in the quantum dot, thus only exist for identical level tunneling ($i=j$). The evaluation of $\mathbf{G}^r$ is straight forward using the Dyson equations which can be expressed in the following matrix inversion that contains the entire composite of system levels:

$$\mathbf{G}^r(\epsilon) = \{[\mathbf{g}^r(\epsilon)]^{-1} - [\mathbf{\Sigma}_L^r(\epsilon) + \mathbf{\Sigma}_R^r(\epsilon)]\}^{-1} \tag{37}$$

and $\mathbf{G}^<$ from the Keldysh equation,

$$\mathbf{G}^<(\epsilon) = \{\mathbf{G}^r(\epsilon)[\mathbf{\Sigma}_L^<(\epsilon) + \mathbf{\Sigma}_R^<(\epsilon)]\mathbf{G}^a(\epsilon)\}. \tag{38}$$

We are interested in the time-averaged current which can be derived from zeroth Fourier component of the Green's functions as

$$I_0 = -\frac{e}{\pi}\mathrm{Im}\int d\epsilon\, \mathrm{Tr} \times\left\{\left[f_L(\epsilon)\mathrm{Re}[\beta(\epsilon)]\mathbf{G}_{00}^r(\epsilon) + \frac{1}{2}\beta^\star(\epsilon)\mathbf{G}_{00}^<(\epsilon)\right]\Gamma_L\tilde{\mathbf{\Sigma}}(\epsilon)\boldsymbol{\sigma}_z\right\}, \tag{39}$$

where the trace over the Nambu space above is adapted in terms of Nambu index as $\mathrm{Tr}\{\mathbf{A}(\epsilon)\}=\{\mathbf{A}_{11}(\epsilon)+\mathbf{A}_{22}(-\epsilon)\}$, and all subsequent analyses are based on time-averaged quantities.

III. RESULTS AND DISCUSSIONS

In order to clearly illustrate the separate effects of level transitions from single-level dynamics, the discussion is organized based on the parameters A and B in Eq. (2). The entire results presented here are for weak-coupling case where $\Gamma=0.04\Delta$, for the reason of key interests explained earlier in the introduction.

A. For $A>0$ and $B=0$

Physically this corresponds to independent absorption and emission of photons by each localized levels in nonequilibrium driven systems. To provide a cleaner picture for such cases we shall confine the discussions only for systems with a single localized level in the quantum dot since the analysis for multilevel systems can be described by superpositions of single-level systems. The results from the Floquet basis using finite matrix truncation exactly resemble the exact analytical solutions using the Bessel basis, and this agreement is attainable even with moderately small Floquet matrix employing ± 4 Fourier terms, suggesting reasonable convergence efficiency of the numerical approach. Smaller frequencies require more Floquet Fourier terms to provide precise picture for the DOS and the current density. In the time-averaged I-V curve of Fig. 2, the current saturation and the steplike features under radiation are similar to Sun *et al.*[9] The dc resonance in general starts to appear whenever the quantum dot level is aligned with the Fermi level for a given bias. However, the main dc resonance at $eV=4\Delta$ originating from the localized level at $\varepsilon_0=-2\Delta$ remains pronounced under the field radiation regardless of its frequency and amplitude. This result differs qualitatively from Sun *et al.*[9] who suggest complete deformation of this dc resonance peak even by moderately low intensity fields ($A\approx\frac{1}{2}\Delta$) using effectively identical system parameters and we believe this is due to inconsistent transforms of the Bessel functions in the Green's function therein. Clearly our results are physically more sensible considering the eigenvalues for those states that do not absorb or emit any photon should remain constant. It is physically more intuitive to visualize zero photon process would always exist at finite probability and therefore would persistently reproduce the dc resonance at the same bias. In atomic systems such as QPCs the charge screening is much weaker, therefore other effects such as spins and Coulombic interactions which are neglected in the current model could potentially shift the resonances positions depending on their interaction strength, as pointed out by Avishai *et al.*[23] who consider full superconducting electrodes with Coulombic repulsion in the quantum dot. Another significant factor is the symmetry of the potential drop across the system which we had already discussed in our earlier works.[24]

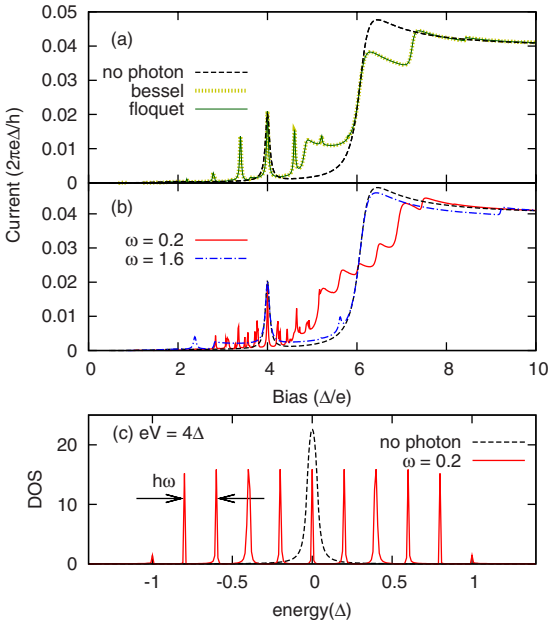

FIG. 2. (Color online) Single-level quantum dot ($A=0.6\Delta$, $\Gamma_L=\Gamma_R=0.04\Delta$, $k_BT=0.1\Delta$, and $\varepsilon_0=-2\Delta$). (a) Time-averaged I-V curve under radiation frequency $\omega=0.6\Delta/\hbar$ showing excellent agreements between analytical and numerical solutions using ± 4 Fourier components. (b) shows the effects of increasing and decreasing radiation frequency at constant amplitude. Spacing between peaks around dc resonance is exactly $\hbar\omega$. (c) Time-averaged DOS at resonant bias ($eV=4\Delta$). The localized level evidently splits into a series of Andreev bound states inside the superconducting gap at uniform interval of $\hbar\omega$.

The secondary resonances occur at various bias equally spaced at $\hbar\omega$ around the dc resonance. The number of secondary resonance increases for smaller frequencies due to more available states in the quantum dot from the harmonics $\varepsilon_p=\varepsilon_0\pm p\hbar\omega$. This is clearly visualized by the equal spacing $\hbar\omega$ between Andreev bound states in the DOS [Fig. 2(c)], where the $\pm p$th resonance may be viewed as p photons absorption or emission process. The widths of these Andreev bound states decrease with their number, conserving the overall DOS and hence the resonance current at this bias. The number of secondary resonances also increases with increasing field amplitude appearing at higher and lower biases due to more contributions from the higher harmonics (higher order photon processes) in the quasistate summations of Eq. (16). For field frequency above the superconducting gap en-

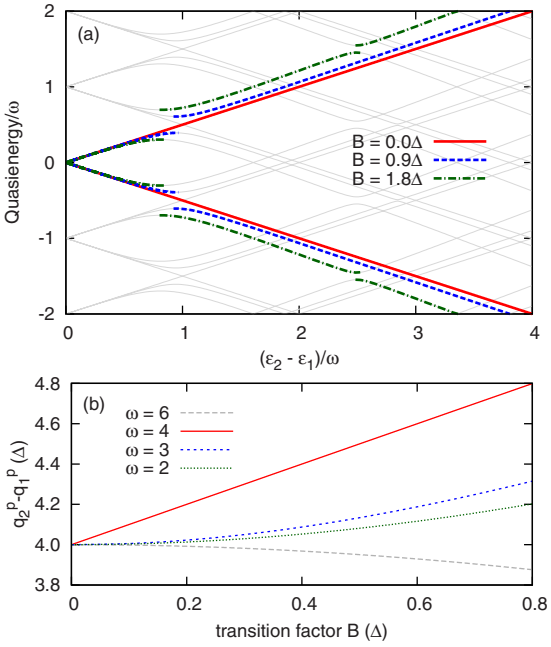

FIG. 3. (Color online) Normalized quasienergy for various coupling factor B of a system with two symmetric localized levels ($\varepsilon_1=-2\Delta$, $\varepsilon_2=2\Delta$, and $A=0$) under zero bias. (a) The zeroth-order quasienergy sets where each branch is associated with the unperturbed localized levels ε_1 and ε_2. The gray background is the nonzero order sets, which form the harmonic infinite set of Floquet quasienergy. (b) Quasienergy difference of pth quasistate for increasing coupling which at Rabi resonance $\omega=(\varepsilon_2-\varepsilon_1)/\hbar$ shows largest difference and behaves in effectively linear fashion with B.

ergy ($\omega>\Delta/\hbar$), the effects start to diminish regardless the localized level's positions relative to the gap since the secondary resonances become too far off the dc resonance, residing either in the region of strong current saturation or in the very small current region where the Andreev bound states are barely above the Fermi level at low bias.

B. For $A=0$ and $B>0$

This corresponds to a quantum dot with two localized levels and oscillatory transition dynamics between the levels. Highlighted in Fig. 3(a) is the normalized zeroth-order quasienergy pair and on the background are the typical infinite sets of harmonic Floquet quasienergy pairs. The upper and lower branches come from the levels above and below Fermi energy, respectively, which are symmetric but the analyses are applicable to general two level systems. Increasing the coupling strength between the two levels introduces increasing quasienergy gap at certain frequencies most significantly at Rabi resonance frequency, $\omega=(\varepsilon_2-\varepsilon_1)/\hbar$, which will be the main interest here since this is a first-order process. In Fig. 3(b), at Rabi frequency the quasienergy difference varies linearly with B and it hardly changes at any other frequencies. The linear relationship between quasienergy difference and coupling strength provides a mechanism to understand the energy distance between singularities in the DOS from harmonic summation in the retarded Green's function [Eq. (16)] which in turn determine the current resonance positions along the bias as illustrated in Sec. III A. Transition dynamics displays distinctly different features from single-level dynamics as shown in Fig. 4 for time-averaged DOS and current density, where multiphoton process of Andreev bound states are now replaced by energy splitting equal to the coupling strength B. As we verify in Figs. 4(a) and 4(b) the DOS at 0 and 4Δ at resonant bias $eV=4\Delta$ would split into two under Rabi frequency, separated by energy difference B due to the increase in quasienergy difference by the same amount. Other radiation frequencies would introduce slight shifts to these densities but not splitting. Similar features visible in the current density J_0 in Figs. 4(c) and 4(d) but the qualitative pictures can never be the same since calculation of J_0 takes into account more complete self-energy effects from the electrodes, making the current density at 0 more diminished in this case.

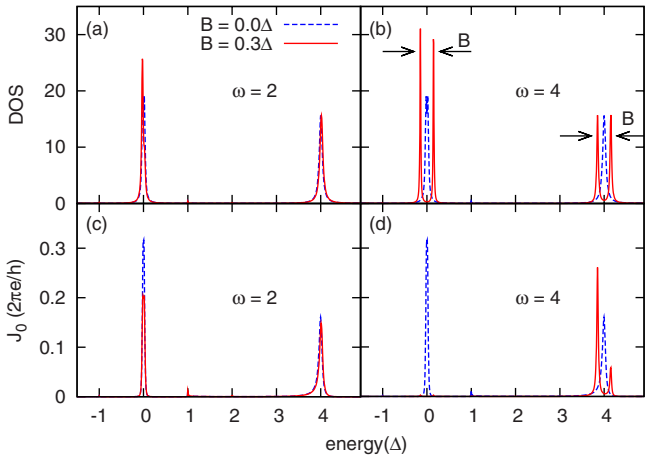

FIG. 4. (Color online) Two-level quantum dot, time-averaged DOS, and current density J_0 at resonant bias $eV=4\Delta$. At this bias, the peak at $\varepsilon=0$ originates from ε_1 and that at $\varepsilon=4\Delta$ from ε_2. When transition between levels is switched on, the qualitative features of the DOS and current density change dramatically at Rabi frequency where there is resonance splitting of the DOS separated by B due to quasienergy change. Complete interaction with the electrodes makes the resonance at $\varepsilon=0$ to diminish in the current density, giving a slight drop of the current at this bias.

The time-averaged I-V curves in Fig. 5 show the effect of radiation on the dc resonance for various frequencies. The dc resonance at $eV=4\Delta$ originates from the localized level $\varepsilon_1=-2\Delta$ while the other level ε_2 is above the Fermi level outside the superconducting gap, therefore contributing current without superconducting resonance features, similar to normal junctions. The ε_2 level would make identical dc resonance at negative bias $eV=-4\Delta$, producing negative current and the complete I-V curve displays the usual antisymmetric form. The resonance splitting in the DOS causes the splitting in the resonance current only at Rabi frequency while other frequencies would hardly change this dc resonance or the entire transport behaviors in general. Around Rabi frequency, the resonance peak splits into two separated by $2B$ and each part starts moving in opposite directions with diminishing magnitude as the coupling strength increases. A slight detuning from the Rabi frequency would produces the same results but with the split pair resonance moves either to the right or

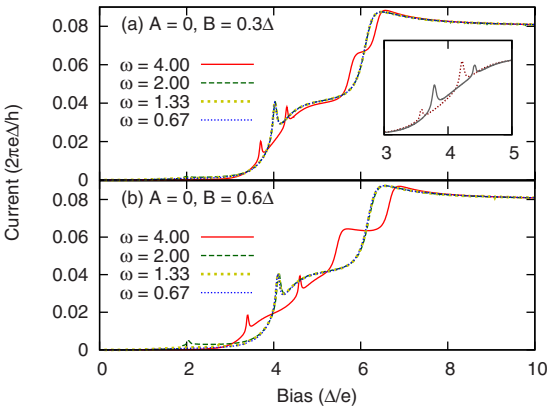

FIG. 5. (Color online) Two level quantum dot ($A=0$, $\Gamma_L=\Gamma_R=0.04\Delta$, $k_BT=0.1\Delta$, $\varepsilon_1=-2\Delta$, and $\varepsilon_2=2\Delta$). At moderate transition factors, only radiation frequency close to Rabi resonance can split the dc resonance ($eV=4\Delta$) into two peaks, separated by interval $2B$. Inset (a), small detuning from Rabi resonance at $\omega=4.1\Delta/\hbar$ (solid black) and $\omega=3.9\Delta/\hbar$ (dashed brown) makes this resonance pair moves to the right and left, respectively, but keeping the separation relatively constant.

to the left as B increases while keeping the separation effectively at $2B$, this can be seen from the inset in Fig. 5(a). In Fig. 6, we again show the effect of increasing coupling and splitting is only effective at Rabi frequency while other frequency only shifts the resonance unless the coupling strength is made unreasonably larger, at which point the dipole model approximation could fail.

We also observe that when the nonharmonic term Q_{ij}^{p} in Eq. (16) is an exact integer ν, the sudden inclusions of the off-diagonal terms in the retarded Green's function do not bring a sudden change in the DOS and current behavior. This suggests a smooth evolution of the DOS and other physical quantities through out the frequency range and various coupling strengths. One reason for the absence of such sudden behavior is these extra off-diagonal terms are higher order processes which tend to be very small by few order of magnitudes compared to the first- and zeroth-order ones, therefore their contributions in the final sum over all quasistates

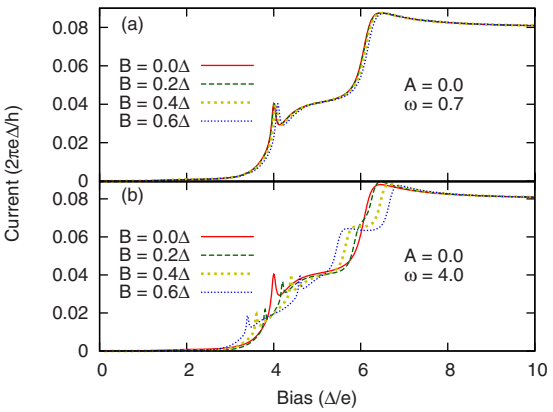

FIG. 6. (Color online) Two-level quantum dot with the same parameters as Fig. 5. (a) No significant changes occur at nonresonant frequency $\omega=0.7\Delta/\hbar$. (b) At Rabi resonant $\omega=4\Delta/\hbar$, the resonance at $eV=4\Delta$ splits up symmetrically separated by interval $2B$.

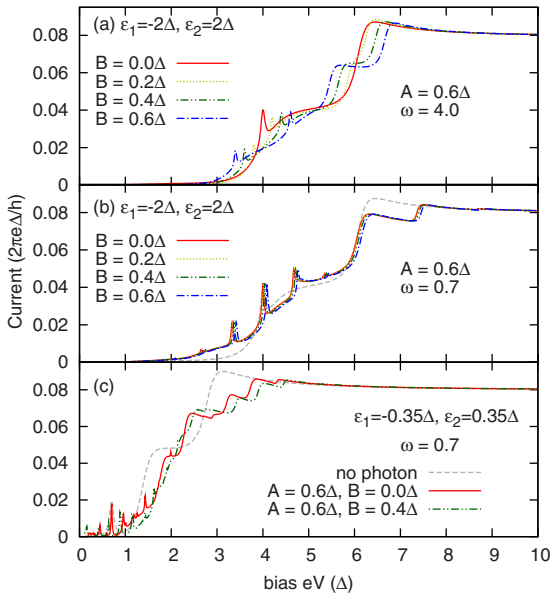

FIG. 7. (Color online) Time-averaged I-V curve for both $A,B>0$. [(a) and (b)] For Level spacing $(\varepsilon_2-\varepsilon_1)=4\Delta$, separate effects from A and B appear at different regions of frequencies. (c) For smaller level spacing $(\varepsilon_2-\varepsilon_1)=0.7\Delta$, the effects from A and B appear on the same frequency.

are never significant. In this semiclassical model, the transition dynamics is thus described effectively by absorption and emission of photon energy determined by the unperturbed localized level spacing $n\hbar\omega=(\varepsilon_2-\varepsilon_1)$ independent on superconducting gap, and therefore for moderate factor B it is only effective for first-order process at Rabi resonance. In the dipole approximation, the coupling strength is simply the matrix element of the perturbation which depends on the electric field polarizations and level orbitals that can be easily measured in isolated quantum dots or atomic ensembles. The current model provides a way to directly measure the coupling matrix elements of a driven tunneling system by measuring the energy separation between the split resonances in the I-V curve.

C. For both $A,B>0$

This is basically the superposition of the two separate cases above, and their noticeable effects may or may not come together in the same frequency region depending on the localized levels spacing of the system. For example, using the quantum dot levels in Sec. III B, $\varepsilon_1=-2\Delta$; $\varepsilon_2=2\Delta$, would display the effects from independent level oscillations and transitions at two very different frequency region, as shown in Figs. 7(a) and 7(b). This is practically expected because the effects from independent level oscillations depend on the superconducting energy gap which tends to be much smaller than energy spacing while the transition effect is dictated by the energy spacing. For example, a low T_C superconducting Nb electrode has an energy gap around ~1.4 meV, compared to a typical InAs or GaAs quantum dot with few tens nanometer diameter that easily have energy spacing in the order of few tens of millielectron volt or larger

between the ground state to the first excited state,[25,26] therefore in general these two effects always appear at separate frequency regions. Also since the interactions are excluded, the model suits better for larger energy spacing, i.e., the more typical quantum dots and the level position of ε_2 in this case become unimportant in affecting independent oscillation dynamics of level ε_1. To illustrate simultaneous effects from the two dynamics in Hamiltonian (2), we must set the localized level spacing to be smaller than the superconducting energy gap as shown in Fig. 7(c) where $\varepsilon_2-\varepsilon_1=0.7\Delta$, however since the model neglects interactions (correlations would be inevitably important at this point), this would serve only as rough qualitative pictures on what would be expected in reality. In Fig. 7(c) we observe the movement of the dc resonance at bias $eV=0.7\Delta$ due to transition dynamics, as well as rich secondary harmonic resonance features with equal spacing $\hbar\omega$ from arbitrary multiphoton process at field frequency $\omega=0.7\Delta/\hbar$.

IV. CONCLUSIONS

We have derived a method for dealing with time-dependent phenomena in transport analysis of an S-N-N mesoscopic junction by incorporating Floquet basis and NEGF framework. The use of Floquet basis and its incorporation into the Green's-function formalism enables more flexible modeling of time-dependent transport. We found that independent level interactions with external fields do not change dc resonance behavior, regardless of the frequency and amplitude of the fields radiation and this differs from the prior theoretical predictions in the literature,[9] accompanied by a series of secondary resonances due to multiphoton processes around the resonance. When the transition between two localized levels is taken into account and level oscillation is neglected, radiations have significant effects only at Rabi resonance when $\omega=(\varepsilon_2-\varepsilon_1)/\hbar$. At Rabi resonance, the main dc resonance splits into two and the separation between them is determined by the coupling strength of the two levels. This model enables the measurements of the coupling strength in such driven system using the *I-V* curve alone.

ACKNOWLEDGMENT

This work is supported by NUS Academic Research Fund (Grants No. R-144-000-237133 and No. R-144-000-255-112).

*phyzc@nus.edu.sg

[1] Y. Meir and N. S. Wingreen, Phys. Rev. Lett. **68**, 2512 (1992).
[2] J. Taylor, H. Guo, and J. Wang, Phys. Rev. B **63**, 245407 (2001); B. Larade, J. Taylor, H. Mehrez, and H. Guo, *ibid.* **64**, 075420 (2001).
[3] M. Octavio, M. Tinkham, G. E. Blonder, and T. M. Klapwijk, Phys. Rev. B **27**, 6739 (1983).
[4] E. N. Bratus', V. S. Shumeiko, and G. Wendin. Phys. Rev. Lett. **74**, 2110 (1995).
[5] D. V. Averin and A. Bardas, Phys. Rev. Lett. **75**, 1831 (1995).
[6] J. C. Cuevas, A. Martin-Rodero, and A. Levy Yeyati, Phys. Rev. B **54**, 7366 (1996).
[7] Q.-F. Sun, H. Guo, and J. Wang, Phys. Rev. B **65**, 075315 (2002).
[8] F. Dolcini and L. Dell'Anna, Phys. Rev. B **78**, 024518 (2008).
[9] Q.-F. Sun, J. Wang, and T.-H. Lin, Phys. Rev. B **59**, 13126 (1999).
[10] S. Shapiro, Phys. Rev. Lett. **11**, 80 (1963).
[11] M. Chauvin, P. vom Stein, H. Pothier, P. Joyez, M. E. Huber, D. Esteve, and C. Urbina, Phys. Rev. Lett. **97**, 067006 (2006).
[12] J. C. Cuevas, J. Heurich, A. Martin-Rodero, A. Levy Yeyati, and G. Schon, Phys. Rev. Lett. **88**, 157001 (2002).
[13] A. Shnirman, G. Schon, and Z. Hermon, Phys. Rev. Lett. **79**, 2371 (1997).
[14] For example, J. Skoldberg, T. Lofwander, V. S. Shumeiko, and M. Fogelstrom, Phys. Rev. Lett. **101**, 087002 (2008); G. Wendin and V. S. Shumeiko, Low Temp. Phys. **33**, 724 (2007), and references therein.
[15] A. Levy Yeyati, J. C. Cuevas, A. Lopez-Davalos, and A. Martin-Rodero, Phys. Rev. B **55**, R6137 (1997).
[16] J. H. Shirley, Phys. Rev. **138**, B979 (1965).
[17] A. Marchenkov, Z. Dai, B. Donehoo, R. N. Barnett, and U. Landman, Nat. Nanotechnol. **2**, 481 (2007); for pioneering in MCBJ, see C. J. Muller, J. M. van Ruitenbeek, and L. J. de Jongh, Phys. Rev. Lett. **69**, 140 (1992).
[18] A. Marchenkov, Z. Dai, C. Zhang, R. N. Barnett, and U. Landman, Phys. Rev. Lett. **98**, 046802 (2007).
[19] S.-H. Ji, T. Zhang, Y. S. Fu, X. Chen, X. C. Ma, J. Li, W. H. Duan, J. F. Jia, and Q. K. Xue, Phys. Rev. Lett. **100**, 226801 (2008); J. K. Gimzewski and R. Moller, Phys. Rev. B **36**, 1284 (1987).
[20] A.-P. Jauho, N. S. Wingreen, and Y. Meir, Phys. Rev. B **50**, 5528 (1994).
[21] C. A. Stafford and N. S. Wingreen, Phys. Rev. Lett. **76**, 1916 (1996).
[22] P. K. Tien and J. P. Gordon, Phys. Rev. **129**, 647 (1963).
[23] Y. Avishai, A. Golub, and A. D. Zaikin, Europhys. Lett. **54**, 640 (2001).
[24] A. Nurbawono, Y. P. Feng, E. Zhao, and C. Zhang, Phys. Rev. B **80**, 184516 (2009).
[25] H. Drexler, D. Leonard, W. Hansen, J. P. Kotthaus, and P. M. Petroff, Phys. Rev. Lett. **73**, 2252 (1994).
[26] E. Scheer, P. Joyez, D. Esteve, C. Urbina, and M. H. Devoret, Phys. Rev. Lett. **78**, 3535 (1997); J. C. Cuevas, A. Levy Yeyati, and A. Martin-Rodero, *ibid.* **80**, 1066 (1998).